tvst

Article

Optimization of the Light Sword Lens for Presbyopia Correction

Walter Torres-Sepúlveda[1], Alejandro Mira-Agudelo[1], John Fredy Barrera-Ramírez[1], Krzysztof Petelczyc[2], and Andrzej Kolodziejczyk[2]

[1] Grupo de Óptica y Fotónica, Instituto de Física, Facultad de Ciencias Exactas y Naturales, Universidad de Antioquia UdeA, Calle 70 No. 52-21, Medellín, Colombia
[2] Faculty of Physics, Warsaw University of Technology, Koszykowa 75, 00-662, Warszawa, Poland

Correspondence: Walter Torres-Sepúlveda, Grupo de Óptica y Fotónica, Instituto de Física, Facultad de Ciencias Exactas y Naturales, Universidad de Antioquia UdeA, Calle 70 No. 52-21 Medellín, Colombia. e-mail: walter.torres@udea.edu.co

Received: June 6, 2019
Accepted: November 11, 2019
Published: February 12, 2020

Keywords: presbyopia; psychophysical assessment; visual optics; optical corrections and treatments

Citation: Torres-Sepúlveda W, Mira-Agudelo A, Barrera-Ramírez JF, Petelczyc K, Kolodziejczyk A. Optimization of the light sword lens for presbyopia correction. Trans Vis Sci Tech. 2020;9(3):6, https://doi.org/10.1167/tvst.9.3.6

Purpose: We propose and evaluate the modifications of a light sword lens (LSL) to obtain better performance for distance vision while maintaining good operation for near and intermediate vision.

Methods: The modifications consisted of assigning angular or circular windows for distance vision while rescaling the LSL profile in the remaining area of the element. The objective performance of the redesigned LSLs was verified numerically by the Strehl ratio and experimentally using correlation coefficients and Michelson contrast. Subjective assessments were provided by monocular visual acuity (VA) and contrast sensitivity (CS) through-focus curves for six patients with paralyzed accommodation. The tested object vergence range was [–4.0, 0.0] diopters (D). All experiments were conducted in a custom-made monocular visual simulator.

Results: Computational simulations and objective experiments confirmed the better performance of the modified LSL for the imaging of distant objects. The proposed angular and radial modulations resulted in flat VA and CS through-focus curves, indicating more uniform quality of vision with clearly improved distance vision. The VA provided by the modified LSL profiles showed a maximal improvement of 1.5 lines of acuity with respect to the VA provided by the conventional LSL at distance vision.

Conclusions: Optimized LSLs provide better imaging of distant objects while maintaining a large depth of focus. This results in comparable and acceptable quality for distance, intermediate, and near vision. Therefore, the modified LSLs appear to be promising presbyopia correctors.

Translational Relevance: The new design of LSL reveals an improved performance for all ranges of vision and becomes a promissory element for a real presbyopia correction in clinical applications.

Introduction

The accommodative amplitude of the human eye progressively decreases with age. This decrease extends from early adolescence to middle adulthood at an average rate of 0.23 diopters (D) per year. The accommodative amplitude reaches its lowest value (approximately 1.00 D) at 55 years of age, and it remains almost constant throughout the remaining old age.[1] This degradation leads to a visual condition known as presbyopia, which is a common refractive pathology that affects a large part of the global population. In 2015, approximately 1.8 billion people had this condition, and it is estimated that 2.1 billion people will develop this condition by 2030.[2] This increase in the number of presbyopic people is expected because life expectancy is currently rising. This increment is evidenced in a similar manner in developed and undeveloped countries, and the population is socially and economically affected. It has been reported that a large percentage of the total global presbyopic population does not use any kind of correction or employs inadequate correction methods.[2,3] This issue about

the visual impairment of the global population had motivated the study and development of mechanisms for the correction of presbyopia, which is a problem that requires attention worldwide.

According to the work of Charman,[4] the ideal correction of presbyopia requires a mechanism or method that must achieve the following features: "capable of restoring to pre-presbyopic levels the dioptric range within which accurate focus can be smoothly and rapidly achieved. It should also be able to maintain this range throughout the remaining decades of the life of the individual, without any further intervention, with the eye always being emmetropic at the lower end of the range." Currently, there are several approaches for correcting presbyopia, including surgical procedures,[5] pharmacological proposals,[6,7] perceptual training,[8] accommodative lenses,[9] and optical methods.[10–12] Even though a large number of approaches have been proposed, evaluated, and implemented, there is not generic and satisfactory solution for the compensation of presbyopia that achieves the requirements of an ideal correction method.

Currently, a common method of correcting presbyopia is denominated modified monovision.[13] This approach consists of the correction of both eyes by the addition of different optical powers, that is, one eye is corrected for near (and/or intermediate) vision and the other for distance vision. These kinds of corrections are typically performed using contact lenses or intraocular lenses. Commonly used contact lenses have multifocal profiles and extended depth of focus (EDOF) profiles.[10,14,15] However, the profiles of contact lenses are frequently refractive with optical power distributed in central and annular zones, which leads to the undesirable dependence of lens performance on pupil size. For this reason, intraocular lenses are used more frequently when monovision is applied.[16,17] Intraocular lenses can be monofocal or multifocal. They allow for the simultaneous imaging of one or more images on the retina, each corresponding to a defined observation distance. Common multifocal lenses are bifocal or trifocal, and they can be refractive or diffractive. Diffractive lenses have the advantage that their performance does not depend strongly on pupil size.[18] In general, two methods are used in the design of multifocal optical elements with added optical power. First, the optical power of the lens is radially distributed; that is, the optical power varies with the distance from the center to the edge of the lens. This results in a strong performance dependence of the elements on the pupil size; this is the most used method currently. In the second method, the distribution of the optical power depends on the angular and radial coordinates simultaneously. Unlike the first method, the performance of the second method is theoretically independent of the pupil size.[19] Several recent works have studied the differences between both types of optical elements, and they have demonstrated that the angular elements provided better optical quality than those with the radial distribution of optical power.[19,20] A recent work compared the optical quality of multifocal optical elements for application in modified monovision. It reported an advantage of bifocal and trifocal angularly segmented elements over elements with radial dependence of the added optical power and over elements with the addition of spherical aberrations. This implies that the combination of multifocal elements with angular distribution of optical power and monovision can enhance the optical performance of elements for presbyopia correction.[21,22]

In the past, intraocular lenses that provide an EDOF of a complete eye–lens system have been proposed.[17] These designs are based on the idea that sharp images are maintained on the retina in an approximately continuous range of object distances. The addition of optical power is continuous across these lenses, which provides suitable performance in an extended range of distances.[23,24]

A few specific optical elements that could be included in the category of lenses that provide an EDOF are axicons,[25] single peacock eye optical elements,[26,27] and light sword lenses (LSLs).[20,28,29] Among these, only LSLs have been studied in subjective experiments or in initial clinical studies for presbyopia compensation.[29,30] An LSL is an asymmetric element with angular variation in the optical power across the complete pupil. To obtain this variation, the element is divided into infinitesimal angular sectors, each with different additions of optical power.[20] According to this, the performance of LSLs does not substantially depend on pupil size,[31,32] which is an advantage with respect to several refractive symmetric profiles of intraocular lenses that are currently used. In a previous study, it was found that LSLs provide satisfactory visual quality in the range of the designed optical power, and their performance declines at the lower and upper ends of this range.[29] It was shown that an LSL designed with the continuous addition of optical power in a range of [0.0, +3.0] D provides appropriate correction for near and intermediate vision (from −2.7 to −0.5 D). However, its performance is not sufficient for both near vision at −3.0 D and distance vision (0.0 D). In distance vision, the decline in correction has been quantified as almost 2.0 lines of acuity compared to the distance-corrected naked eye.[29] This issue represents the major drawback of LSLs with respect to other methods for presbyopia correction. For

this reason, the issue must be overcome to achieve the actual application of LSLs.

The asymmetric profile of LSL design causes a radially asymmetrical point spread function (PSF). This asymmetry, along with the blur produced by the superimposition of out-of-focus images and a sharp image, can affect the performance of LSLs in a different manner compared to conventional symmetric PSFs. According to Wolffsohn and Davies,[13] the presence of blur can affect the contrast sensitivity (CS) provided by an LSL. In a recent study, the CS provided by an LSL designed in the form of a refractive lens was evaluated.[30] It was found that the CS is acceptable for object vergences of 0.3 D and 2.5 D. However, it is necessary to evaluate the complete range of object vergences (from 33 cm to infinity) to obtain a complete evaluation of the contrast properties offered by an LSL element and the different modified LSL profiles proposed in this work.

In this study, we optimize the transmittance function that defines the phase profile of an LSL to improve the performance of the LSL at distance vision. Our optimization consists of assigning an area of the optical element corresponding only to distance vision and rescaling the profile in the remaining area of the element. The optimization process is developed and evaluated in three stages, i.e., computational simulations, optical bench experiments, and psychophysical measurements; the last one consists of the examination of the visual acuity (VA) and CS provided by the LSL and the proposed modified LSL profiles. This study attempts to evaluate the optimized LSLs as elements for correcting presbyopia in the complete range of functional vision.

Methods

Modified Transmittance Functions of the LSL

The LSL provides an angular modulation of optical power for generating an EDOF. This modulation is continuous, with different infinitesimal angular sectors contributing linearly to different optical powers.[20,29,30] The phase transmittance function that describes this LSL phase profile is expressed as follows:

$$\varphi(r,\theta) = \frac{P_{max} r^2(\theta)}{4\pi}, \tag{1}$$

where r and θ are polar coordinates and P_{max} denotes the maximum optical power addition in a range of $[0, P_{max}]$. Henceforth, this phase profile will be referred to as the conventional LSL profile. The profile defined by this function has not shown appropriate visual performance corresponding to distance vision.[29,30] Therefore, by utilizing the focusing geometry of the LSL, it is necessary to propose the modifications of the above conventional transmittance function to enhance distant vision.

The first modification of the conventional transmittance function is carried out by considering that the focusing geometry of the LSL allows for the selection of a desired optical power and for the reinforcement of the LSL performance by enlarging the size of the corresponding angular sector. Thus, the modification consists of assigning an angular window with zero optical power, while the modulation of optical power in a range of $(0, P_{max}]$ is rearranged within the remaining area of the element (see the first row of Fig. 1). Therefore, the new phase transmittance function obtained in this manner is given by the following equation:

$$\varphi(r,\theta,\beta) = \begin{cases} 0, & \theta < \beta \\ \frac{P_{max} r^2(\theta-\beta)}{2(2\pi-\beta)}, & \beta \le \theta \le 2\pi, \end{cases} \tag{2}$$

where β is the size of the angular window, and the remaining variables are the same as those in Equation 1. Henceforth, the phase profiles obtained through this angular modification will be referred to as aLSL profiles.

The second method of obtaining a modified LSL is to substitute the above angular window by a central circular window with zero optical power, while the conventional profile is rearranged in the remaining annular zone (see the second row in Fig. 1). The phase transmittance function obtained in this manner is expressed by the following equation:

$$\varphi(r,\theta,\alpha) = \begin{cases} 0, & r \le \alpha R; \\ \frac{P_{max}\theta\left(r^2-(\alpha R)^2\right)}{4\pi\left(1-\alpha^2\right)}, & \alpha R < r \le R \end{cases} \tag{3}$$

where α is the fraction of the LSL's radius, R, assigned to the circular window (with $0 \le \alpha < 1$). The remaining variables are the same as those in Equation 1. Henceforth, the phase profiles obtained through this radial modification will be referred to as rLSL profiles.

The aim of the present work is to study the modified LSLs to obtain suitable profiles (determined by β or α values) that would provide better distance vision without considerable decline in near and intermediate vision, as compared to the performance of the conventional LSL profile.

Eight modified LSL profiles were proposed and tested. There were four LSL profiles corresponding to angular modifications with windows sizes of 30°, 45°, 60°, and 90° (parameter β in Equation 2) and four LSL profiles with radial modifications corresponding to α

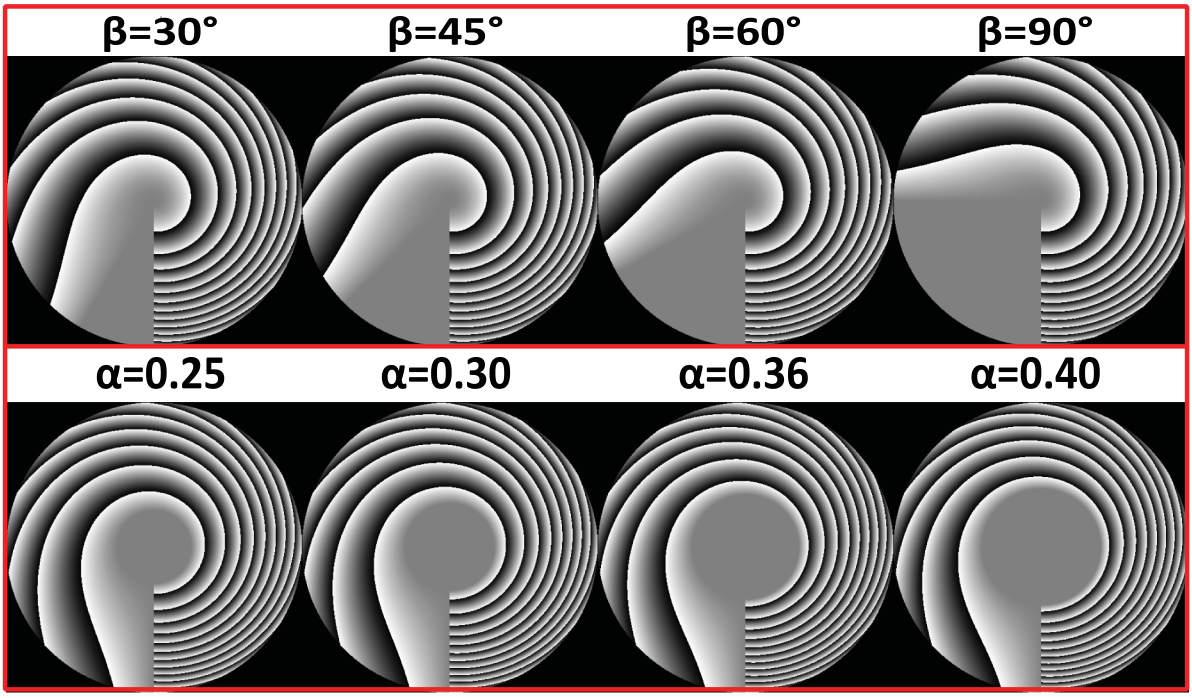

Figure 1. Top row: angularly modified LSL (aLSL) profiles. Bottom row: radially modified LSL (rLSL) profiles. The gray scale of the images denotes the wrapped phase transmittance of each element.

values of 0.25, 0.30, 0.36, and 0.40 (see Equation 3). The phase profiles of the evaluated elements are shown in Figure 1, with their corresponding window sizes. All LSL profiles had $P_{max} = +3.0$ D, which provided modulation in an optical power range of [0.0, +3.0] D.

Computational Simulations

Fourier optics was used for simulating the performance of the modified LSL profiles. The Strehl ratio computed in the frequency domain (SRMTF) using a modulation transfer function (MTF) was used as the optical quality metric.[33] The MTF is the magnitude of an optical transfer function that is defined by the Fourier transform of the incoherent PSF obtained from the Fourier transform of the generalized pupil describing an evaluated system.[34] The SRMTF was calculated as the integration of the MTF provided by the evaluated element normalized by the integration of the MTF provided by a diffraction-limited system.

$$\text{SRMTF} = \frac{\iint_{-\infty}^{+\infty} \text{MTF}\left(f_x, f_y\right) df_x df_y}{\iint_{-\infty}^{+\infty} \text{MTF}_{D-L}\left(f_x, f_y\right) df_x df_y}. \quad (4)$$

Computational simulations were performed for LSL profiles with a pupil diameter of 4.10 mm. This pupil diameter was based on the corresponding values used in the objective and subjective experiments. Generalized pupils corresponding to a monofocal system and conventional and modified LSL profiles were designed to build SRMTF through-focus curves. The tested defocus (object vergence) range was [−4.0, 0.0] D in steps of 0.5 D. Calculations were carried out on a square matrix of size 8192 × 8192 pixels with a sufficiently small sampling of 1.22 µm per pixel.

Optical Bench Experiments

Objective and subjective experiments were performed using a monocular visual simulator (MVS).[35] The experimental system is shown in Figure 2. The MVS was a combination of the following optical elements: an imaging lens (IL), a spatial light modulator (Pluto-SLM), a Hartmann–Shack wavefront sensor (HSS: complementary metal–oxide–semiconductor camera with resolution of 1024 × 1280 pixels and 200-µm microlens pitch with 7-mm focal length; Flexible OKO Optical, Rijswijk, The Netherlands), and an artificial pupil (AP). Pluto-SLM was a reflective liquid-crystal-on-silicon spatial light modulator (phase-only, PLUTO-NIR; Holoeye Photonics AG, Berlin, Germany) with full high-definition resolution and a pixel pitch of 8.00 µm. These elements were located in different conjugated planes through different afocal systems consisting of achromatic doublet pairs. The MVS measured different visual quality parameters using a polychromatic stimulus pathway

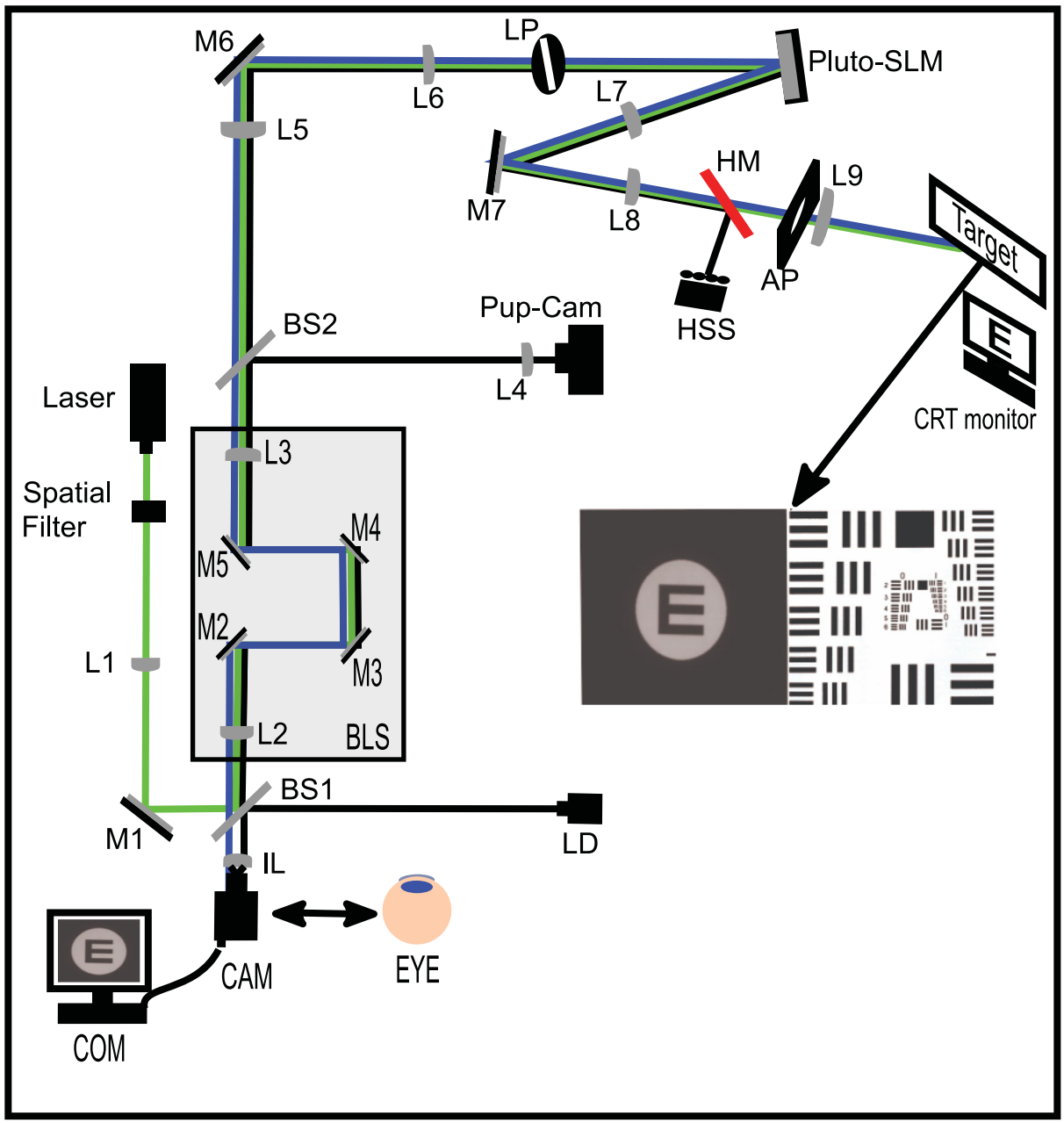

Figure 2. MVS setup. Laser: 532-nm wavelength; spatial filter: microscope objective and pinhole. AP, artificial pupil; BLS, Badal lens system; BS, beam splitter; CAM, charge-coupled-device (CCD) Sony camera; COM, computer; CRT, cathode-ray tube computer; HM, hot mirror; HSS, Hartmann–Shack wavefront sensor; IL, imaging lens; L, lens; LD, laser diode; LP, linear polarizer; M, mirror; Pluto-SLM, PLUTO-NIR spatial light modulator; Pup-Cam, pupil camera.

(blue line). Stimuli were generated in two manners: with a cathode-ray tube (CRT) monitor with a resolution of 192 pixels per degree located 2.52 m behind the AP or using translucent targets located at the focal plane of a collimating lens (L9) with a focal length of 75.00 cm placed extremely close to the AP. The AP was the entrance pupil of the system, which determined the effective pupil size of the system and the appropriate illumination of the optical elements located at each conjugated plane.

The MVS measured the ocular aberrations using the HSS and a laser diode (980-nm wavelength, black line in Figure 2; 60-μW maximum power on the IL and patient's pupil plane). Lenses L2 and L3 with a focal length of 15.00 cm and mirrors M2–M5 created a Badal lens system (BLS) that induced a desired object vergence in a range of -5.0 to $+5.0$ D. The BLS also maintained the same angular size of the images projected on the CRT monitor. The IL was an achromatic doublet lens with a focal length of 7.50 cm, and

it was located at a distance of 15.00 cm from lens L2. CAM was a charge-coupled device (CCD) monochromatic Sony camera (model XCL-U1000) with a resolution of 1598× 1199 pixels, pixel pitch of 4.40 µm, and bit depth of 16.

The MVS had a total magnification of 0.75× (in the direction from the IL to the CRT monitor) because achromatic lenses L5 and L6 had focal lengths of 20.00 cm and 15.00 cm, respectively. Additionally, the afocal system, comprising achromatic lenses L7 and L8, had a magnification of 1× because they had the same focal length (20.00 cm). The AP was a physical circular pupil with diameter of 3.06 mm, which corresponded to a diameter of 4.08 mm at the patient's pupil plane owing to the magnification of the system. The LSL phase profiles shown in Figure 1 were projected on Pluto-SLM with a diameter of 4.54 mm for obtaining a size of 6.00 mm on the IL (or patient's pupil) plane. The radially modified LSL profiles had windows with diameters of 1.50 mm ($\alpha = 0.25$), 1.80 mm ($\alpha = 0.30$), 2.16 mm ($\alpha = 0.36$), and 2.40 mm ($\alpha = 0.40$) on the patient's pupil plane. The LSL profiles were emulated as contact lenses because Pluto-SLM was located at a conjugated plane of the MVS entrance pupil. The laser and the remaining optical elements shown in Figure 2 were used for the alignment and calibration of the setup.

The imaging with the single IL and with the combined system of the IL and the projection of the nine LSL phase profiles (including the conventional profile) on Pluto-SLM was studied. Two targets were used in the objective experiments. The first was a black Snellen optotype "E" inside a white circle, as shown in Figure 2. The image of this target had an angular size of 3.15° on the CCD camera measured from the IL plane, while the width of a bar of the Snellen optotype had an angular size of 0.29° measured from the same plane. The second was a US Air Force resolution test (USAF test) with groups of bars corresponding to different spatial frequencies on the image plane. Both targets were located at the focal plane of collimating lens L9, and they were back-illuminated with auxiliary polychromatic light (white LEDs), which is not shown in Figure 2.

Two metrics derived from output images were used. The first was the calculation of the correlation coefficient (CC), which was defined as follows[36]:

$$\mathrm{CC} = \frac{\sum_m \sum_n \left(A_{mn} - \bar{A}\right)\left(I_{mn} - \bar{I}\right)}{\sqrt{\left(\sum_m \sum_n \left(A_{mn} - \bar{A}\right)^2\right)\left(\sum_m \sum_n \left(I_{mn} - \bar{I}\right)^2\right)}}, \tag{5}$$

where $\bar{A}$ and $\bar{I}$ are the average pixel values of the images to be correlated, and A_{mn} and I_{mn} are the image values at pixel coordinates (m, n). Image I corresponds to a reference image, while A corresponds to the output images of the Snellen optotype to be compared.

The images obtained by the IL adjusted to infinity, by the conventional LSL, and by the modified LSL profiles were recorded by CAM. CC through-focus curves were built in a range of object vergences of [−4.0, 0.0] D in steps of 1.0 D. The images to be correlated corresponded to the target of the Snellen optotype. The reference image was obtained with the monofocal IL adjusted at infinity for an object vergence of 0.0 D and without any profile projected on Pluto-SLM. All images of the optotype were centered before the calculation of the CC.

The second metric used for evaluating the performance of the modified LSL profiles was the Michelson contrast (MC), which is defined by Equation 6.[34] The MC was calculated from the output images of the USAF test recorded by CAM. The set of bars selected on the USAF images corresponded to a spatial frequency of 7.5 lines/mm on the CCD camera plane. MC through-focus curves were built for the monofocal system (without any profile projected on Pluto-SLM) and for the nine studied LSL profiles. The object vergence range was the same as that tested in the previous metric. The MC is defined as follows:

$$\mathrm{MC} = \frac{I_{max} - I_{min}}{I_{max} + I_{min}}, \tag{6}$$

where I_{max} and I_{min} are the maximum and minimum pixel values of an image, respectively.

The quality of imaging was examined based on the proposed objective metrics by utilizing the modified phase profiles of the LSL. This objective study enabled us to determine the most useful LSL profiles to be tested in the subjective experiments described below.

Psychophysical Experiments

VA and CS were measured in six patients with paralyzed accommodation. The patient's pupil was located in the IL plane using the pupil camera shown in Figure 2. VA and CS were measured for the naked eye and for the eye compensated by the phase profile of the conventional LSL and by three modified LSL profiles: two corresponding to angular modification (aLSL with $\beta = 45°$ and 90°) and one with radial modification (rLSL with $\alpha = 0.36$). These profiles were selected because they exhibited better performance in the objective experiments (see Results section). The six patients were aged between 24 and 39 years, with a mean age of 29 ± 6 years. The patients had healthy eyes without any

previous ocular surgery. Exclusion criteria consisted of patients with an astigmatism magnitude of over 0.5 D. Accommodation was paralyzed with two drops of 1% tropicamide ophthalmic solution to induce an accommodative amplitude similar to that of an old presbyopic eye. VA and CS were measured monocularly in the dominant eye of the patients, which was determined using the hole-in-the-card test. The nondominant eye was occluded with a patch. The pupil size of all patients was larger than 6.80 mm, which implies that the AP was the only element that limited the light entering the eye. Informed consent was obtained from the patients after explaining the nature and possible consequences of the study. The study was approved by the Bioethics Committee of the University Research Center (Sede de Investigación Universitaria) from the University of Antioquia, Medellín, Colombia. The measurement protocols followed the tenets of the Declaration of Helsinki.[37]

It was possible to measure the ocular aberrations of the patients using the HSS and LD. Additionally, the subjective refraction of the patients was corrected by the BLS. The ocular aberration measurements quantified the average astigmatism (-0.4 ± 0.2 D) in a range of [−0.5, −0.1] D and determined that the limit of the exclusion criterion of –0.5 D was not exceeded. Astigmatism and high-order aberrations were not corrected. The average refraction was -0.5 ± 1.3 D in a range of [−2.7, 0.4] D. The average root mean square of the high-order aberration (until fifth order) was 0.10 ± 0.02 µm based on a pupil diameter of 6.00 mm. The average best-corrected distance visual acuity (BCDVA) was -0.06 ± 0.02 in a range of −0.10 to −0.04 presented in the logMAR scale.

The measurement protocol started with the determination of the dominant eye, the application of the first drop of 1% tropicamide ophthalmic solution, and the alignment of the patient's pupil with the optical axis of the MVS. A bite bar was used to maintain the alignment of the patient's eye. After the alignment, the second drop of the ophthalmic solution was applied. Then, the best focus (subjective refraction) was obtained using the BLS. The best focus corresponded to the 0.0-D defocus of the patient. Ocular aberrations were measured at this BLS position. First, VA and CS were measured for the naked eye (no compensated eye) using the CRT computer monitor and the Freiburg Vision Test software (FrACT).[38] Each VA value was the average of two series of measurements performed using FrACT, consisting of 30 projections of tumbling Snellen optotype "E" with different sizes and orientations. The CS value was the average of two series of measurements performed using FrACT, consisting of 30 projections of Landolt optotype "C" with a constant angular size of 50 arcminutes and a gap of 10 arcminutes on a patient's pupil plane but with variation in the contrast level and orientation. This method was similar to the Pelli–Robson contrast sensitivity test, which is commonly used for the rapid determination of CS.[39] The average output luminance of the CRT monitor was 126 cd/m^2. The evaluated object vergences were {−4.0, −3.0, −2.0, −1.0, −0.5, 0.0} D. After the measurements for the naked eye, the conventional LSL and the three modified phase profiles of the LSL were projected on Pluto-SLM, and VA and CS were measured. Measurements were performed in two sessions corresponding to VA and CS. Each session required two hours after the application of the second drop of ophthalmic solution. After the first hour in each session, the third drop of ophthalmic solution was applied, and the patients rested for 10 minutes. The sessions for measuring VA and CS were conducted on different days.

Results

Computational Simulations and Optical Bench Experiments

Figure 3 shows the simulated SRMTF through-focus curves obtained with the different phase profiles of the LSL. The black line corresponds to a monofocal system, while the blue line corresponds to the conventional LSL phase profile. Both SRMTF through-focus curves are shown with the modified LSL profiles for the purpose of comparison.

From Figure 3, the decrease in the SRMTF with the magnitude of the object vergence in the monofocal system is noticeable, which is the expected behavior for a fixed-focus system. The maximum value of the SRMTF was equal to 1 at 0.0 D, and it decreased until a value of 0.006 at –4.0 D. The blue curve shows the behavior of the SRMTF obtained by the conventional LSL. As it was anticipated, there were lower SRMTF values at the upper and lower ends of the designed optical power range (–3.0 and 0.0 D). The SRMTF had a value of 0.122 at 0.0 D with its maximum equal to 0.264 at –1.5 D.

The results shown in Figure 3a correspond to the SRMTF through-focus curves obtained by the aLSL profiles. It is clear that, for these modified LSL profiles, the SRMTF presented higher values at 0.0 D than that obtained by the conventional LSL. Additionally, for the rest of the optical powers of the designed range, the aLSL profiles kept the feature of providing an EDOF but with lower SRMTF values than those obtained for the conventional LSL. The SRMTF values determined

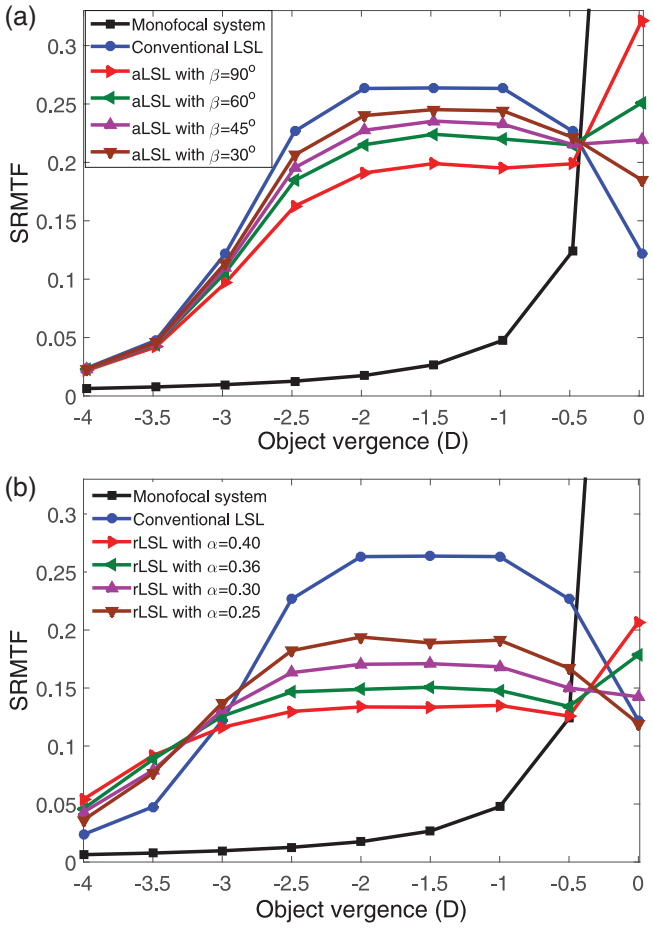

Figure 3. Simulated SRMTF though-focus curves computed in a monofocal system, using a conventional LSL profile. (a) aLSL profiles with $\beta = 90°, 60°, 45°$, and 30° and (b) rLSL profiles with $\alpha = 0.40, 0.36, 0.30$, and 0.25. The black line (monofocal system) had a maximum value equal to 1 at 0.0 D.

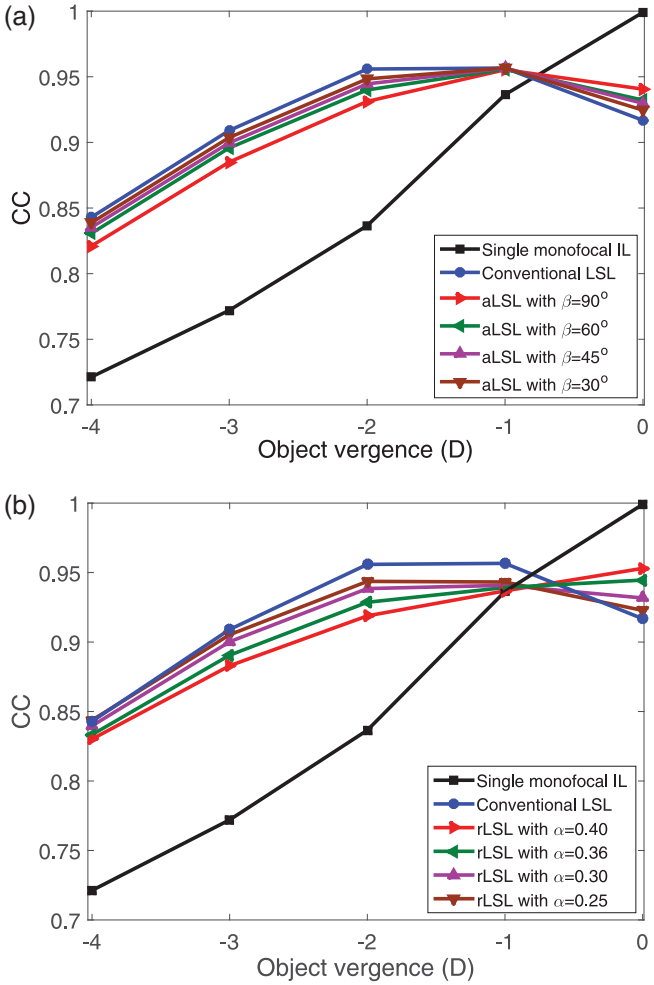

Figure 4. Experimental CC through-focus curves obtained from output images of the Snellen optotype formed by a single monofocal IL, by a conventional LSL profile and (a) by aLSL profiles with $\beta = 90°, 60°, 45°$, and 30° and (b) by rLSL profiles with $\alpha = 0.40, 0.36, 0.30$, and 0.25.

at 0.0 D were equal to 0.322, 0.251, 0.219, and 0.185 for angular sizes of 90°, 60°, 45°, and 30°, respectively.

On the other hand, Figure 3b shows the SRMTF through-focus curves corresponding to the modified LSL with radial windows. At 0.0 D, similar to the angular case, it is possible to observe SRMTF values increasing with dimensions of the windows. For windows corresponding to α equal to 0.40, 0.36, 0.30, and 0.25, SRMTF values of 0.207, 0.179, 0.142, and 0.119, respectively, were obtained. Additionally, the rest of the SRMTF values in the designed range were approximately constant but smaller than the values provided by the conventional LSL profile.

From a comparison of Figures 3a and 3b, a difference between the SRMTF curves corresponding to the aLSL and rLSL profiles can be seen. Generally, aLSL profiles generate higher SRMTF values in the designed range [–3.0, 0.0] D. Thus, numerical simulations based on the SRMTF metric suggest that aLSL profiles have an advantage over rLSL profiles.

Continuing with the evaluation of the optimization process of the LSL profiles, Figure 4 shows the CC through-focus curves computed from the experimental output images of the Snellen target. Figures 4a and 4b correspond to the curves obtained by the aLSL and rLSL profiles, respectively.

From Figure 4, the expected behavior of the CC values provided by the single monofocal IL adjusted to infinity (black line) can be seen. The maximum CC value was 1 at 0.0 D, with a progressive decrease when the magnitude of the object vergence became larger, reaching a CC value of 0.721 at –4.0 D. The blue line corresponds to the CC through-focus curve provided by the conventional LSL profile, which shows a tendency similar to that obtained in the SRMTF case with CC = 0.917 at 0.0 D.

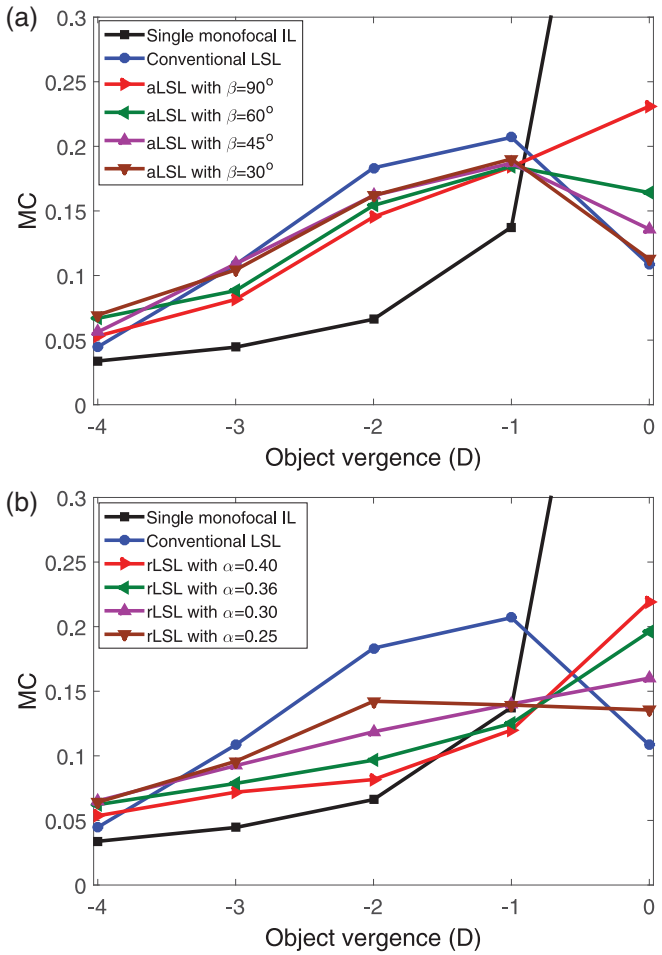

Figure 5. Experimental MC through-focus curves from output images of the USAF test imaged by a single monofocal IL, by the conventional LSL profile and by (a) aLSL profiles with $\beta = 90°$, 60°, 45°, and 30° and (b) rLSL profiles with $\alpha = 0.40$, 0.36, 0.30, and 0.25.

Figure 4 shows that all modified profiles improve CC at 0.0 D compared to the conventional LSL. Particularly, the angular modification results in CC values of 0.941, 0.932, 0.930, and 0.925 for $\beta = 90°$, 60°, 45°, and 30°, respectively (Fig. 4a). The radial modification provides similar CC values equal to 0.953, 0.945, 0.932, and 0.923 for $\alpha = 0.40$, 0.36, 0.40, and 0.25, respectively (Fig. 4b). Moreover, in the object vergence range [–4.0, –1.0] D for both modulations, values slightly smaller than those provided by the conventional LSL are noticeable.

The experimentally obtained CC through-focus curves shown in Figure 4 confirm the computational simulations (Fig. 3), particularly in the trends of the curves and the improved performance at 0.0 D.

The final objective experimental assessment of the imaging provided by the modified LSL profiles was made by measuring the MC of the USAF test images. The results are shown in Figure 5.

In Figures 5a and 5b, the black line denotes the MC through-focus curve obtained by the single monofocal IL, which has a maximum value of 0.705 at 0.0 D and a decreasing behavior until the lowest MC value of 0.034 at –4.0 D. The blue line indicates the MC through-focus curve obtained by the conventional LSL profile. In general, it exhibits the same tendency as the CC and the SRMTF curves obtained for the conventional LSL profile.

MC through-focus curves for the aLSL profiles are shown in Figure 5a. The curves indicate higher MC values at 0.0 D (0.231, 0.164, 0.136, and 0.113, respectively) than the conventional LSL in the same object vergence (0.108). Figure 5b shows the MC through-focus curves obtained by the rLSL profiles. As in the angular case, there were high MC values at 0.0 D resulting in the following values: 0.219, 0.196, 0.160, and 0.135.

In the object vergence range [–3.0, –1.0], the aLSLs provide slightly lower MC values than the conventional LSL. On the other hand, these values are generally higher than the respective ones corresponding to rLSLs.

From the results of computational simulations and objective evaluation described above, three LSL profiles were chosen to perform the psychophysical measurements, namely, two aLSL profiles with $\beta = 90°$ and 45° and one rLSL profile with $\alpha = 0.36$. These profiles exhibited better performance across the previous assessments, with a clear improvement at 0.0 D and providing an EDOF in the rest of optical power within the range [–3.0, –0.5] D. The aLSL profile with $\beta = 90°$ was selected because of its highest values at 0.0 D obtained by the SRMTF and MC metrics, while the profiles with $\beta = 45°$ and $\alpha = 0.36$ were chosen because their performance at 0.0 D was better than that of the conventional LSL profile without overly compromising their performance in the range [–3.0, –0.5] D.

Psychophysical Results

To evaluate the performance of the modified LSL profiles to correct presbyopia in real patients, the VA and CS were measured by compensating a naked presbyopic eye with the proposed modified LSL profiles. The average VA through-focus curves obtained from the six patients are shown in Figure 6.

The black line shows the typical behavior of the VA for a distance-corrected naked eye with low accommodative amplitude, consisting of the best VA value obtained at 0.0 D and a monotone worsening when object vergence is induced. In a logMAR scale, the average BCDVA was -0.06 ± 0.02 and the worst VA value was 0.76 ± 0.13 obtained at -4.0 D. This worst

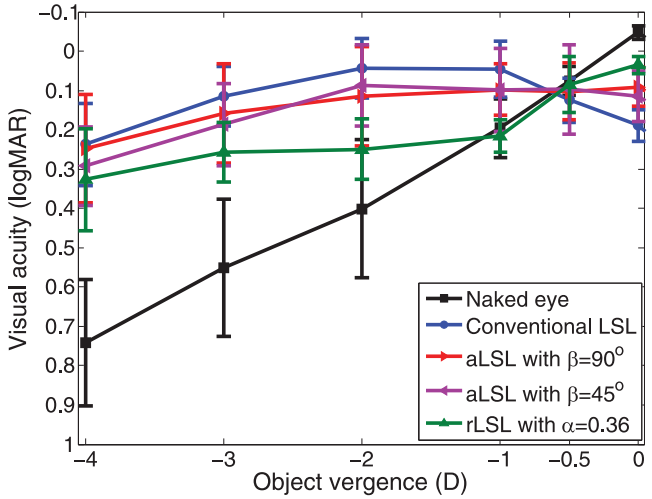

Figure 6. Average VA through-focus curves obtained for the naked eye (black line), the eye compensated by the conventional LSL profile (blue line), the aLSL profiles with $\beta = 90°$ (red line), $\beta = 45°$ (magenta line), and by the rLSL profile with $\alpha = 0.36$ (green line). The VA is presented in an inverted logMAR scale. The error bars represent one standard deviation (±1.0 SD) of the VA values obtained for the six patients in each object vergence.

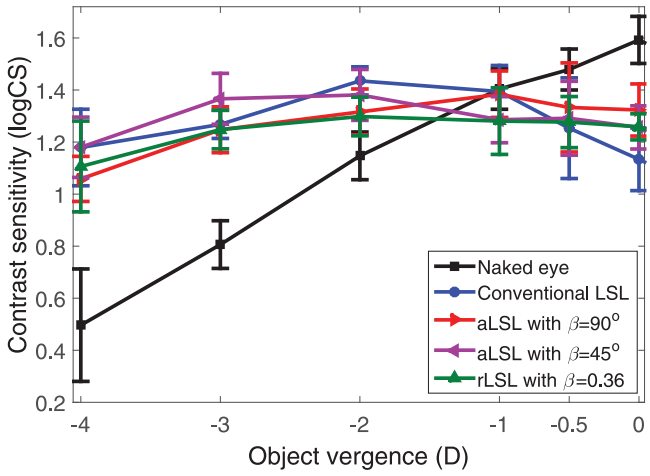

Figure 7. Average CS through-focus curves obtained for the naked eye (black line), the eye compensated by the conventional LSL profile (blue line), by the aLSL profiles with $\beta = 90°$ (red line), $\beta = 45°$ (magenta line), and by the rLSL profile with $\alpha = 0.36$ (green line).The error bars represent one standard deviation (±1.0 SD) of the CS values obtained for the six patients in each object vergence.

VA value represents 16% of BCDVA (this and the next percentual comparations are calculated in a normalized decimal scale).

The blue line represents the average VA through-focus curve for the eye compensated by the conventional LSL profile. The EDOF provided by the LSL is noticeable, with better VA values than those obtained with the naked eye in the range of [–4.0, –1.0] D. At –0.5 D, the same VA value as that found for the naked eye was obtained, and finally at 0.0 D, the decreasing of VA was found.[29] The average VA value at 0.0 D was 0.19 ± 0.04, while the average VA value was 0.08 ± 0.04 calculated in the remaining object vergences in the designed optical power range, that is, in the range [–3.0, –0.5] D. These VA values correspond to 57% and 74% of BCDVA, respectively.

The red and magenta lines represent the VA through-focus curves obtained for the aLSL profiles with $\beta = 90°$ and $\beta = 45°$, respectively. In both cases, there were higher VA values at 0.0 D with respect to that obtained for the conventional LSL profile. According to the previous results of computational simulations and optical bench experiments, there were lower average VA values in the range [–3.0, –1.0] D, while at –0.5 D, all curves matched. The VA curves corresponding to both aLSL profiles were similar. The mean VA values at 0.0 D were 0.09 ± 0.06 and 0.11 ± 0.05 for profiles with $\beta = 90°$ and $\beta = 45°$, which represent 72% and 68% of BCDVA, respectively. Additionally, the average VA values calculated across the object vergence range [–3.0, –0.5] D were 0.12 ± 0.03 and 0.12 ± 0.05 for $\beta = 90°$ and $\beta = 45°$, respectively, representing 69% of BCDVA.

Finally, the green line represents the average VA through-focus curve obtained for the rLSL profile with $\alpha = 0.36$. As well as for the aLSL profiles, the central radial window provided a higher VA value at 0.0 D than that of the conventional LSL profile. This VA value equal to 0.03 ± 0.02 represents 82% of BCDVA, and it was also better than those obtained with the aLSL profiles. Figure 6 confirms the conclusions from computational simulations and objective experiments that the performance of the radial profiles is worse than that of the angular ones in the object vergence range [–4.0, –1.0] D. The average VA value calculated across the object vergence range [–3.0, –0.5] D was 0.20 ± 0.08, corresponding to 57% of the BCDVA.

According to Figure 6, all modified elements present a remarkable advantage for distance vision over the conventional LSL profile. The elements improve VA by approximately 25% at 0.0 D with a moderate average drop of the VA values in the object vergence range [–3.0, –0.5] D.

The last assessment of the modified LSL profiles (Fig. 7) shows the average CS through-focus curves in a logarithmic scale, measured for the naked eyes, and the eyes compensated by the LSLs.

The black line represents the CS measurements obtained for the naked eye. CS clearly decreases with the magnitude of the induced object vergence. The highest CS value was 1.59 ± 0.09 at 0.0 D, while the lowest CS value was 0.5 ± 0.2 at –4.0 D. That is, 9% of the CS value was obtained at 0.0 D (in a

normalized decimal scale). On the other hand, the blue line corresponds to the CS through-focus curve provided by the conventional LSL profile. As in the cases of previously evaluated metrics, the EDOF is clear in the object vergence range [–3.0, 0.0] D, with a small decrease in CS at –3.0 and 0.0 D. The CS value at 0.0 D was 1.13 ± 0.12, while the average CS value calculated across the object vergence range [–3.0, –0.5] D was 1.34 ± 0.09. These values represent 35% and 58% of the CS value obtained for the naked eye at 0.0 D.

The effect of the modified LSL profiles over the CS is depicted by the red, magenta, and green curves. The red line represents the CS through-focus curve generated by the aLSL profile with $\beta = 90°$. This curve depicts the highest CS value among all the tested LSL profiles at 0.0 D. It also exhibits a small decrease in the CS values in the optical power range of [–4.0, –1.0] D with respect to the conventional LSL profile. The mean CS value at 0.0 D was 1.32 ± 0.10, and the average CS value calculated across the object vergence range [–3.0, –0.5] D was 1.32 ± 0.06. These CS values represent 54% of the CS value corresponding to that of the naked eye at 0.0 D. The aLSL profile with $\beta = 45°$ generated a similar CS through-focus curve represented by the magenta line. The mean CS value at 0.0 D was 1.26 ± 0.08, and an average value of CS calculated across the object vergence range [–3.0, –0.5] D was equal to 1.33 ± 0.05. These values represent 46% and 56% of the CS value, respectively, for the naked eye at 0.0 D. Finally, the green line denotes the CS through-focus curve corresponding to the rLSL profile. A flatter shape of the curve can be seen, with small variations in the designed object vergence range [–3.0, 0.0] D. The mean CS value at 0.0 D was the same as that obtained for the aLSL profile with $\beta = 45°$ (1.26 ± 0.05). Additionally, an average CS value of 1.28 ± 0.02 was calculated across the rest of the designed optical power range [–3.0, –0.5] D. These values represent 46% and the 49% of the CS value obtained for the distance-corrected naked eye.

Discussion

Computational simulations and optical bench experiments demonstrated the proper functionality of the proposed modifications of the LSL profiles. First, there was an improvement in the distant imaging performed by all the modified LSL profiles. This improvement generally increased with sizes of the windows designed for distance vision. Second, the proposed modifications did not affect the performance of the LSL considerably, conserving EDOF in the designed range of the optical power. Finally, it was found that, in the object vergence range [–4.0, –1.0] D, corresponding to near and intermediate vision, the modified LSL profiles exhibited substantial advantages over the monofocal system, regardless of the evaluated objective metrics. Thus, the modified LSL profiles are apparently useful for presbyopia compensation, as it was reported for the conventional LSL profile.[29,30]

Table. One-Way ANOVA from Results of Figures 6 and 7[a]

Correction Condition	*P* Value for VA	*P* Value for CS
Naked eye	7.149×10^{-16}	4.097×10^{-24}
Conventional LSL	5.400×10^{-6}	1.552×10^{-5}
aLSL with $\beta = 90°$	0.3587	0.0975
aLSL with $\beta = 45°$	0.1095	0.0378
rLSL with $\alpha = 0.36$	2.086×10^{-12}	0.7638

[a]The test allows the comparison of each mean VA value (and mean CS values) obtained in the object vergence range [–3.0, 0.0] D, as it is provided by each correction condition. The significance level was 0.05.

According to Figures 6 and 7, the subjective psychophysical experiments confirm the features described above. Some small differences between the computational simulations and optical bench experiments occurred due to the use of different metrics. While SRMTF through-focus curves were obtained from the numerically simulated PSF, the CC and MC through-focus curves were computed from experimental output images. We obtained a good match between trends of the curves predicted by the objective metrics and the psychophysical measurements.

To compare the ability of the proposed modified LSL profiles for presbyopia compensation, a one-way analysis of variance (ANOVA) and pairwise comparison using a Tukey-Kramer test with a significance level of 0.05 (5%) were performed on the psychophysical results.

Initially, we applied the one-way ANOVA test to each VA and CS through-focus curve shown in Figures 6 and 7. Table shows the *P* values obtained in each case.

First, we carried out the one-way ANOVA for analyzing VA. For the naked eye, a *P* value of 7.149×10^{-16} was found, confirming our expectation that the VA values obtained in the range [–3.0, 0.0] D were statistically different. The *P* value 5.400×10^{-6} obtained for the VA curve of the conventional LSL profile indicated that the VA values were also statistically different. Particularly, with a post hoc pairwise analysis, it was found that the VA values at 0.0 and –0.5 D had significant differences with the other VA

values of other object vergence values, supported in P values lower than 0.0432. On the other hand, P values of 0.3587 and 0.1095 obtained for the VA values provided by the aLSL profiles with $\beta = 90°$ and $\beta = 45°$, respectively, imply that the measured VA values were not statistically different in the evaluated object vergence range, which coincides properly with the red and magenta curves in Figure 6. Finally, the P value 2.086×10^{-12} indicates that the rLSL profile generates at least one mean VA value being substantially different from the other VA values. According to the pairwise analysis, these different VA values were found at 0.0 and –0.5 D, leading to P values lower than 0.0010 when they were compared with the other VA values. This finding is well illustrated in Figure 6.

The third column of Table shows the P values obtained from the CS curves shown in Figure 7. For the naked eye, a P value of 4.097×10^{-24} confirms statistically significant differences between all measured CS values. The analysis of the conventional LSL profile leads to the P value of 1.552×10^{-5} and to a similar conclusion. The P value obtained for the aLSL with $\beta = 90°$ was 0.0975, which indicates that there were no significant differences in the total object vergence range. A P value equal to 0.0378 was obtained for the aLSL with $\beta = 45°$. Although in this case, the P value of the one-way ANOVA test indicated statistically significant differences, a pairwise analysis showed that there were no significant differences among all measured mean CS values. The pairwise P values from all possible comparisons were higher than 0.0684. Finally, the P value of 0.7638 confirms the flat shape of the CS through-focus curve provided by the rLSL in Figure 7.

The presented results of the one-way ANOVA test and pairwise comparison confirm EDOF properties of the modified LSL profiles, including near, intermediate, and distance vision. This result contrasts with the findings for the conventional LSL profile, where distance vision is clearly impaired.

An additional comparison with the pairwise methodology was made. In this case, either the mean VA or CS values obtained at each object vergence for all evaluated profiles were compared. This comparison is important, especially for distance vision corresponding to an object vergence of 0.0 D, where we expect the differences and improvements of the psychophysical metrics.

The obtained results show that, in the range [–4.0, 0.0] D, the VA values obtained for the naked eye were generally statistically different from those generated by all the LSL profiles, with P values lower than 0.0131. The exceptions were obtained at –0.5 D, as at this particular object vergence, all the VA values sufficiently coincided (P values larger than 0.6359) at –1.0 D, where there was a significant difference only with respect to the conventional LSL, expressed by a P value of 0.0039.

The pairwise analysis also revealed that, in the object vergence range [–4.0, –0.5] D, the VA values provided by all the LSL profiles did not show significant differences, with P values larger than 0.0529. The only exception is the rLSL showing some differences with the other profiles at the object vergence values of –2.0 and –1.0 D, providing P values lower than 0.0114.

Similar analysis was made for the CS through-focus curves. At almost all object vergence values in the range [–4.0, 0.0] D, the CS values obtained for the naked eye were statistically different from those obtained with the LSL profiles, with P values lower than 0.0045. Exceptions were found at –1.0 D, where all CS values sufficiently matched (P values larger than 0.0543), and at –0.5 D, where there were differences only with the modified LSL profiles (P value lower than 0.0412).

The analysis also revealed that, in the object vergence range [–4.0, –0.5], there are no substantial differences among all analyzed LSLs.

What is particularly important in the case of the object vergence 0.0 D connected with distance vision is that the test showed significant differences between measured VA and CS after using the modified LSL profiles instead of the conventional LSL profile. The P values were lower than 0.0028 and 0.0348 for the VA and CS results, respectively.

The above statistical comparison illustrates substantial changes in presbyopic vision after correction by the LSL profiles. The obtained results confirm the noticeable improvement in distance vision by the modified elements compared to the conventional LSL. Moreover, according to our analysis of VA and CS, generally there are no significant differences between correction performed by all LSLs in the object vergence range [–4.0, –0.5] D. The only evident exception is VA reduced by the radial profile at the object vergence values of –2.0 and –1.0 D. This slight difference in the rLSL performance coincides well with the objective predictions of the computational simulations and optical bench experiments. Despite the above disadvantage of the rLSL, our findings show the usefulness of the modified LSLs. Substitution of the conventional LSL by modified profiles leads to more uniform EDOF performance. The distance vision is clearly enhanced without noticeable declination of near and intermediate vision.

According to available references, Figure 8 compares the VA through-focus curves provided by

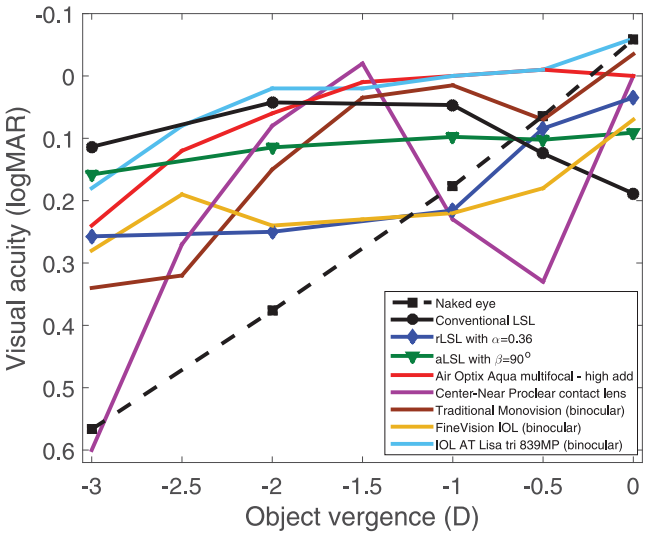

Figure 8. Average VA through-focus curves obtained by different methods for correcting presbyopia.

the analyzed LSLs and by other corrections of presbyopia. We analyzed the following correctors: a contact lens, Air Optix Aqua Multifocal with high addition (Alcon, Dallas, TX)[40]; a center-near Proclear multifocal contact lens (Coopervision, Pleasanton, CA)[41]; the simulated compensation by the conventional monovision (binocular simulator)[42]; an intraocular lens (IOL), diffractive trifocal IOL FineVision (PhysIOL, Liège, Belgium)[43]; and a diffractive trifocal IOL, AT Lisa tri 839MP (Carl Zeiss Meditec AG, Oberkochen, Germany).[44]

Figure 8 shows the serious drawback of the conventional LSL reducing distance vision quality. Although the advantage of the conventional LSL for near and intermediate vision over almost all other approaches is clear, it exhibits poorer performance for distance vision. On the other hand, the aLSL and rLSL profiles considerably improve distance vision, keeping similar quality of near and intermediate vision. For 0.0 D, the conventional LSL profile results in a drop of 2.4 lines of acuity compared with that for the naked eye; the aLSL and rLSL cause a loss of only 1.5 and 0.9 lines of acuity, respectively. Differences between the aLSL and other solutions at 0.0 D are following: the aLSL causes a maximum difference of 1.5 lines of acuity compared to AT Lisa tri 839MP IOL (cyan line) and a minimum difference of 0.2 lines compared to the IOL FineVision (yellow line). Similarly, the rLSL causes a maximum difference of 0.9 lines of acuity with respect to AT Lisa tri 839MP IOL, and it exhibits better performance than the IOL FineVision with 0.4 lines of acuity over it. The rest of the compared corrector elements showed an average advantage of 1.0 and 0.5 lines of acuity over the VA provided at 0.0 D by the aLSL and rLSL, respectively.

Data available in the literature also permit a comparison of CS provided in distance and near vision by the analyzed LSLs and two different contact lenses designed for presbyopia correctors. It is possible to see that the Acuvue Oasys contact lenses for presbyopia (Johnson & Johnson, New Brunswick, NJ),[45] PureVision multifocal contact lenses (Bausch & Lomb, Rochester, NY),[45,46] and the modified LSL profiles generate comparable CS values.

The presented comparisons of the LSLs with commercially available correctors confirm the usefulness of the modified profiles for presbyopia correction. Particularly, the proposed LSL modifications improve distance vision, while a substantial range of EDOF is maintained. It must be noted that the curves and the values corresponding to commercial solutions (Fig. 8) were obtained with elements tested binocularly. It is known that, in general, binocular measurements provide better values than monocular ones. This means that the VA and CS values obtained for the LSLs should be higher if binocular experiments are conducted.

On the other hand, the performance of the rLSL depends on the pupil size. Thus, aLSL exhibits an advantage over rLSL because the applied angular window maintains the independence of geometry focusing from the pupil size.[31,32] However, rLSL compensates this drawback with a better performance for distance vision than aLSL.

The present study confirms the abilities of the modified LSL for presbyopia correction. Proposed modifications substantially enhance distance vision, which becomes comparable with near and intermediate vision. Although the obtained results appear very promising, the practical applications of the modified elements as contact lenses or particularly as intraocular lenses require further investigations. Notably, binocular measurements should be made to obtain additional general knowledge about the abilities and advantages of the modified LSL profiles for ophthalmic applications, particularly for presbyopia compensation. In this sense, it is important to simulate several correction conditions using the strategy of modified monovision, which could contribute to the better performance of the LSL profiles at 0.0 D and a smaller decrease in their performance for the rest of the optical powers. Also, experiments in different conditions should be carried out, such as evaluation of the visual outcomes in mesopic and scotopic illumination to assess the response of the LSL profiles in night conditions. Furthermore, experiments for low-contrast visual acuity assessments, stereopsis study, and so on

should be considered. Additionally, from this preliminary conceptual knowledge about the properness of the modified LSL profiles as elements that compensate for presbyopia, it is necessary to develop similar experiments with real people with presbyopia. In people with presbyopia, other features must be evaluated to understand the interaction between the modified LSL profiles and other conditions of the visual system, such as the senile miosis and the dispersion of light by the ocular media.

Finally, the relation between the optical aberrations and the phase profile of the LSL has remarkable importance. It is known that the optimal orientation of asymmetric multifocal profiles as those with angularly segmented zones is influenced by the ocular aberration.[22] In a recent work, it was found that the optimal orientation of the profile and the coma and spherical aberrations have a beneficial influence on the monocular and binocular performance of multifocal elements. Similarly, the behavior of the asymmetric profile of the LSL is expected to be affected by the orientation of the angular windows and aberrations of the patient's eye. This can be useful in improving the performance of the LSL. However, in the present work, we did not correct ocular aberrations and located the angular windows of the aLSL with a defined orientation. Therefore, additional work must be conducted to control the orientation of the angular windows of the aLSL, which would improve its performance for presbyopia correction. This study should be the next step in the optimization procedure, where typical aberrations of real people with presbyopia can be used, and a complete study on the relations between optical aberrations and LSL phase profile can be established, using a methodology similar to the one proposed by de Gracia and Hartwig.[22]

Conclusions

In this work, we proposed and evaluated different modifications of the LSL, enhancing its ability for presbyopia compensation. Computational simulations, optical bench experiments, and psychophysical measurements demonstrated that the proposed modifications provide a significant improvement in objective distant imaging and presbyopia compensation at distance vision. The subjective experiments confirmed the results of objective metrics as the Strehl ratio, correlation coefficient, and Michelson contrast. According to the performed psychophysical tests, the visual acuity and the contrast sensitivity obtained via the modified LSLs do not vary substantially; that is, the modified profiles lead to a more uniform EDOF performance. Therefore, the radial and angular modifications maintain the vision with a large depth of focus, with distance vision distinctly better than in the case of the use of the conventional LSL. The presented comparisons revealed the slight advantages of the angular profiles over the radial ones, as the aLSLs provide better intermediate and near vision. Moreover, the aLSL profiles are less sensitive to changes in pupil size.[32] Despite these differences, the comparisons of the modified LSL with commercially available presbyopia correctors show similar quality of vision, resulting in comparable VA and CS values.

These findings allow us to conclude that the proposed modified LSLs appear very promising for presbyopia compensation in the complete range of functional vision, corresponding to object vergences from 0.0 to –4.0 D. The modified LSL profiles are also suitable in applications that require objective imaging with a very large depth of focus.

However, it is necessary to consider that the present work is the first conceptual step toward starting a set of trials, determining the effectiveness of the modified LSLs for presbyopia correction. It means that it is necessary to conduct a more complete study involving real patients with presbyopia, binocular assessment, modified monovision, and low-luminance evaluations.

Acknowledgments

Supported by grants from Comité para el Desarrollo de la Investigación (CODI) of the Universidad de Antioquia UdeA, Fondo Francisco José de Caldas (Colciencias-Colombia, grant 727 of 2015; W. Torres-Sepúlveda), and the Polish National Centre for Research and Development (NCBiR) under grant PBS/A9/23/2013 within the framework of the strategic scientific research and experimental development program "Model of Intraocular Lens Providing Extended Depth of Field" (A. Kolodziejczyk and K. Petelczyc).

Disclosure: **W. Torres-Sepúlveda**, None; **A. Mira-Agudelo**, None; **J.F. Barrera-Ramírez**, None; **K. Petelczyc**, None; **A. Kolodziejczyk**, None

References

1. Charman WN. Non-surgical treatment options for presbyopia. *Expert Rev Ophthalmol*. 2018;13:219–231.

2. Fricke TR, Tahhan N, Resnikoff S, et al. Global prevalence of presbyopia and vision impairment from uncorrected presbyopia: systematic review, meta-analysis, and modelling. *Ophthalmology*. 2018;125:1492–1499.
3. Holden BA, Tahhan N, Jong M, et al. Towards better estimates of uncorrected presbyopia. *Bull World Health Organ*. 2015;93:667.
4. Charman WN. Virtual issue editorial: presbyopia—grappling with an age-old problem. *Ophthalmic Physiol Opt*. 2017;37:655–660.
5. Charman WN. Developments in the correction of presbyopia II: surgical approaches. *Ophthalmic Physiol Opt*. 2014;34:397–426.
6. Crawford KS, Garner WH, William B. Dioptin^{TM}: a novel pharmaceutical formulation for restoration of accommodation in presbyopes. *Invest Ophthalmol Vis Sci*. 2014;55:3765.
7. Benozzi J, Benozzi G, Orman B. Presbyopia: a new potential pharmacological treatment. *Med Hypothesis, Discov Innov Ophthalmol*. 2012;1:3.
8. Sterkin A, Levy Y, Pokroy R, et al. Vision improvement in pilots with presbyopia following perceptual learning. *Vision Res*. 2017;113:62.
9. Alió JL, Alió del Barrio JL, Vega-Estrada A. Accommodative intraocular lenses: where are we and where we are going. *Eye Vis*. 2017;4:16.
10. Bakaraju RC, Ehrmann K, Ho A. Extended depth of focus contact lenses vs. two commercial multifocals: Part 1. Optical performance evaluation via computed through-focus retinal image quality metrics. *J Optom*. 2018;11:10–20.
11. De Vries NE, Nuijts RMMA. Multifocal intraocular lenses in cataract surgery: literature review of benefits and side effects. *J Cataract Refract Surg*. 2013;39:268–278.
12. Schallhorn SC, Teenan D, Venter JA, et al. Monovision LASIK versus presbyopia-correcting IOLs: comparison of clinical and patient-reported outcomes. *J Refract Surg*. 2017;33:749–758.
13. Wolffsohn JS, Davies LN. Presbyopia: effectiveness of correction strategies. *Prog Retin Eye Res*. 2018;68:124–143.
14. Bakaraju RC, Tilia D, Sha J, et al. Extended depth of focus contact lenses vs. two commercial multifocals: Part 2. Visual performance after 1 week of lens wear. *J Optom*. 2017;11:21–32.
15. Kim E, Bakaraju RC, Ehrmann K. Power profiles of commercial multifocal soft contact lenses. *Optom Vis Sci*. 2017;94:183–196.
16. Iida Y, Shimizu K, Ito M. Pseudophakic monovision using monofocal and multifocal intraocular lenses: hybrid monovision. *J Cataract Refract Surg*. 2011;37:2001–2005.
17. Auffarth GU, Hagen PR. Multifocal intraocular lenses and extended depth of focus intraocular lenses. *Asia Pacific J Ophthalmol*. 2017;6:339–349.
18. Alió JL, Tavolato M, De La Hoz F, Claramonte P, Rodríguez-Prats JL, Galal A. Near vision restoration with refractive lens exchange and pseudoaccommodating and multifocal refractive and diffractive intraocular lenses: Comparative clinical study. *J Cataract Refract Surg*. 2004;30:2494–2503.
19. de Gracia P, Dorronsoro C, Marcos S. Multiple zone multifocal phase designs. *Opt Lett*. 2013;38:3526–3529.
20. Kakarenko K, Ducin I, Grabowiecki K, et al. Assessment of imaging with extended depth-of-field by means of the light sword lens in terms of visual acuity scale. *Biomed Opt Express*. 2015;6:1738–1748.
21. de Gracia P. Optical properties of monovision corrections using multifocal designs for near vision. *J Cataract Refract Surg*. 2016;42:1501–1510.
22. de Gracia P, Hartwig A. Optimal orientation for angularly segmented multifocal corrections. *Ophthalmic Physiol Opt*. 2017;37:610–623.
23. Millán MS, Vega F. Extended depth of focus intraocular lens chromatic performance. *Biomed Opt Express*. 2017;8:4294–4309.
24. Cochener B. Clinical outcomes of a new extended range of vision intraocular lens: International Multicenter Concerto Study. *J Cataract Refract Surg*. 2016;42:1268–1275.
25. Ares J, Flores R, Bara S, Jaroszewicz Z. Presbyopia compensation with a quartic axicon. *Optom Vis Sci*. 2005;82:1071–1078.
26. Romero LA, Millañ MS, Jaroszewicz Z, Kolodziejczyk A. Double peacock eye optical element for extended focal depth imaging with ophthalmic applications. *J Biomed Opt*. 2012;17:046013.
27. Torres-Sepúlveda W, Barrera JF, Henao R, et al. Imaging with an extended depth of field by means of the peacock eye optical element. *Photonics Lett Pol*. 2017;9:128–130.
28. Kolodziejczyk A, Bará S, Jaroszewicz Z, Sypek M. The light sword optical element—a new diffraction structure with extended depth of focus. *J Mod Opt*. 1990;37:1283–1286.
29. Mira-Agudelo A, Torres-Sepúlveda W, Barrera JF, et al. Compensation of presbyopia with the light sword lens. *Investig Ophthalmol Vis Sci*. 2016;57:6870–6877.
30. Petelczyc K, Byszewska A, Chojnacka E, et al. The light sword lens—a novel method of

presbyopia compensation: pilot clinical study. *PLoS One*. 2019;14:e0211823.
31. Petelczyc K, Garcia JA, Bará S, et al. Presbyopia compensation with a light sword optical element of a variable diameter. *Photonics Lett Pol*. 2009;1:55–57.
32. Torres-Sepúlveda W, Mira-Agudelo A, Barrera JF, Kolodziejczyk A. Experimental evaluation of light sword lens performance with a variable pupil size. *Photonics Lett Pol*. 2018;10:36–38.
33. Thibos LN, Hong X, Bradley A, Applegate RA. Accuracy and precision of objective refraction from wavefront aberrations. *J Vis*. 2004;4:9.
34. Goodman JW. *Introduction to Fourier Optics*. 2nd ed. New York, NY: McGraw-Hill Series in Electrical and Computer Engineering; 1996.
35. Fernández EJ, Manzanera S, Piers P, Artal P. Adaptive optics visual simulator. *J Refract Surg*. 2002;18:S634–S638.
36. Fisher RA. *Statistical Methods for Research Workers*. 5th ed. Edinburgh: Oliver and Boyd; 1934.
37. World Medical Association. World Medical Association Declaration of Helsinki: ethical principles for medical research involving human subjects. *J Am Med Assoc*. 2013;310:2191–2194.
38. Bach M. The Freiburg visual acuity test—variability unchanged by post-hoc re-analysis. *Graefe's Arch Clin Exp Ophthalmol*. 2007;245:965–971.
39. Pelli DG, Robson JG, Wilkins AJ. The design of a new letter chart for measuring contrast sensitivity. *Clin Vis Sci*. 1988;2:187–199.
40. Plainis S, Ntzilepis G, Atchison DA, Charman WN. Through-focus performance with multifocal contact lenses: effect of binocularity, pupil diameter and inherent ocular aberrations. *Ophthalmic Physiol Opt*. 2013;33:42–50.
41. Legras R, Benard Y, Rouger H. Through-focus visual performance measurements and predictions with multifocal contact lenses. *Vision Res*. 2010;50:1185–1193.
42. Schwarz C, Manzanera S, Prieto PM, Fernández EJ, Artal P. Comparison of binocular through-focus visual acuity with monovision and a small aperture inlay. *Biomed Opt Express*. 2014;5:3355.
43. Sheppard AL, Shah S, Bhatt U, Bhogal G, Wolffsohn JS. Visual outcomes and subjective experience after bilateral implantation of a new diffractive trifocal intraocular lens. *J Cataract Refract Surg*. 2013;39:343–349.
44. Mojzis P, Peña-García P, Liehneova I, Ziak P, Alió JL. Outcomes of a new diffractive trifocal intraocular lens. *J Cataract Refract Surg*. 2014;40:60–69.
45. Madrid-Costa D, Gracía-Lázaro S, Albarrán-Diego C, Ferrer-Blasco T, Montés-Micó R. Visual performance of two simultaneous vision multifocal contact lenses. *Ophthalmic Physiol Opt*. 2013;33:51–56.
46. Gupta N, Naroo SA, Wolffsohn JS. Visual comparison of multifocal contact lens to monovision. *Optom Vis Sci*. 2009;86:98–105.